

Nanoscale Phase Segregation in Supramolecular π -Templating for Hybrid Perovskite Photovoltaics from NMR Crystallography

Michael A. Hope,[◇] Toru Nakamura,[◇] Paramvir Ahlawat,[◇] Aditya Mishra,[◇] Manuel Cordova, Farzaneh Jahanbakhshi, Marko Mladenović, Rashmi Runjhun, Lena Merten, Alexander Hinderhofer, Brian I. Carlsen, Dominik J. Kubicki, Renana Gershoni-Poranne, Thomas Schneeberger, Loï C. Carbone, Yuhang Liu, Shaik M. Zakeeruddin, Janusz Lewinski, Anders Hagfeldt, Frank Schreiber, Ursula Rothlisberger,* Michael Grätzel,* Jovana V. Milić,* and Lyndon Emsley*



Cite This: *J. Am. Chem. Soc.* 2021, 143, 1529–1538



Read Online

ACCESS |



Metrics & More

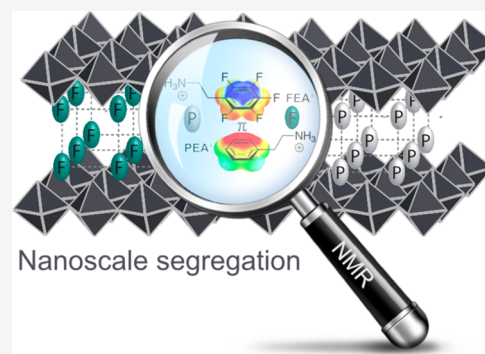


Article Recommendations



Supporting Information

ABSTRACT: The use of layered perovskites is an important strategy to improve the stability of hybrid perovskite materials and their optoelectronic devices. However, tailoring their properties requires accurate structure determination at the atomic scale, which is a challenge for conventional diffraction-based techniques. We demonstrate the use of nuclear magnetic resonance (NMR) crystallography in determining the structure of layered hybrid perovskites for a mixed-spacer model composed of 2-phenylethylammonium (PEA⁺) and 2-(perfluorophenyl)ethylammonium (FEA⁺) moieties, revealing nanoscale phase segregation. Moreover, we illustrate the application of this structure in perovskite solar cells with power conversion efficiencies that exceed 21%, accompanied by enhanced operational stability.



INTRODUCTION

Hybrid perovskite photovoltaics rival other solar cell technologies with their high performance at competitive cost. These systems are based on the AMX₃ composition that defines a corner-sharing crystal structure (such as the cubic lattice shown in Figure 1a) consisting of A cations, mainly Cs⁺, methylammonium (MA⁺, CH₃NH₃⁺), or formamidinium (FA⁺, CH(NH₂)₂⁺), as well as their mixtures, along with divalent M cations (such as Pb²⁺ and Sn²⁺) and halide anions (I⁻, Br⁻, Cl⁻).^{1–3} Their photovoltaic performances and widespread adoption are, however, compromised by limited stability. This can result in degradation due to reactivity with oxygen and water as well as internal ion migration under operating conditions of voltage bias and light irradiation.^{1,4,5} One of the emerging strategies to address these instabilities is based on the incorporation of layers of hydrophobic organic cations between the hybrid perovskite slabs to form layered two-dimensional (2D) perovskites. One example of this approach is the Ruddlesden–Popper perovskite phases based on the S₂A_{n-1}M_nX_{3n+1} composition, where S⁺ is a spacer cation (Figure 1b).^{6–9} These materials have shown greater resilience to degradation, yet their photovoltaic performance is impaired by the poor electronic properties of the spacer layers and by the lack of ordered supramolecular packing, which impedes overall crystallinity.^{6,7,10} The interactions between the organic moieties that form the spacer layer directly affect the structure

of the resulting materials and, consequently, their optoelectronic properties.^{6,11} While progress has been made in the search for new organic moieties that can form layered perovskites, their assembly can only be controlled by having a thorough understanding of the noncovalent interactions which direct the supramolecular structure, such as hydrogen bonding,^{12–15} van der Waals interactions,^{9,16} metal coordination,¹⁷ halogen bonding,^{18,19} and π -based interactions.^{20–23} Furthermore, to unravel these interactions, it is vital to accurately determine the atomic structure. This is a challenge for conventional diffraction techniques, due to polycrystallinity and the presence of heavy atoms.²¹

Solid-state nuclear magnetic resonance (NMR) spectroscopy has previously been used to determine the local structure of hybrid perovskites and their composites with various organic molecules.^{24–27} In particular, NMR crystallography, where the structure is determined by comparing the experimental NMR parameters to those calculated for trial structures, is a powerful

Received: November 3, 2020

Published: January 14, 2021



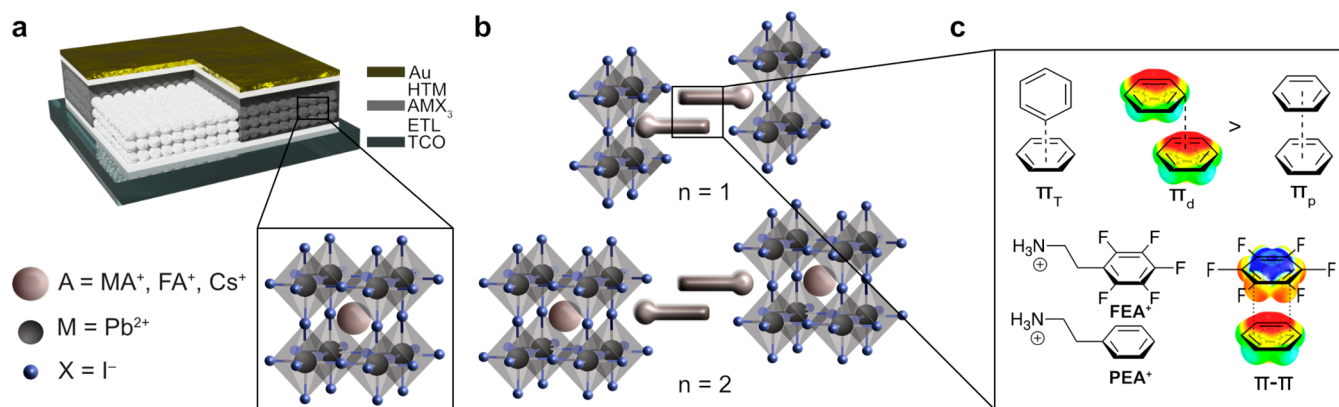


Figure 1. Supramolecular material design. (a) Schematic of the perovskite solar cell with the hybrid perovskite absorber material (AMX₃). HTM = hole transporting material; ETL = electron transporting layer; TCO = transparent conductive oxide. (b) Schematic representation of the structure of Ruddlesden–Popper phases of hybrid 2D perovskites based on the S₂A_{n-1}M_nX_{3n+1} formula ($n = 1, 2$, etc.) comprised of an organic spacer (S⁺) bilayer. (c) Top: Overview of possible π – π interaction modes between two arenes with comparable electron-density surfaces, with different interaction strengths ($\pi_T \approx \pi_d > \pi_p$). Lower: Arene–fluoroarene π – π interaction (π_p) and the spacer cations used in this study: PEA⁺ and FEA⁺. The π_p and π_d interactions of model systems are illustrated by the corresponding ESP maps (also shown in Figure S4 of the SI).

tool for analyzing the organic assemblies and their templating effects in hybrid perovskite materials.^{19,28}

One of the most widely employed organic moieties for layered perovskites is 2-phenylethylammonium (PEA⁺; Figure 1c), which interacts with the hybrid perovskite slabs via ion pairing and hydrogen bonding through the ammonium termini (–NH₃⁺).^{9,20,21,29} The assembly of the organic layer is directed by weaker van der Waals and π -based interactions between the organic moieties (Figure 1c),^{11,20,30} which determine the relative orientation of the aromatic rings according to their quadrupole moments.^{31,32} The quadrupole moment of a benzene ring and the corresponding dispersion interactions stabilize two orientations, T-shaped (π_T) and parallel displaced (π_d), which are more favorable than the parallel orientation (π_p ; Figure 1c, top).³² This is due to areas of positive and negative potential of the aromatic core, which can be visualized by the electronic density distribution or electrostatic potential (ESP) maps (Figure 1c and Figure S4, Supporting Information (SI)). Fluoroarenes, such as 2-(perfluorophenyl)ethylammonium (FEA⁺, Figure 1c), feature a reversed quadrupole moment due to the higher electronegativity of fluorine substituents, which favors parallel π interactions (π_p) in benzene–perfluorobenzene systems (Figure 1c, bottom).³² Parallel π – π stacking of the spacer cations could thus, in principle, be directed by employing alternating arene–fluoroarene moieties.^{21,31} In addition, the presence of fluoroarene moieties could further contribute to the hydrophobicity of the material, improving its resilience to moisture, while fluoroarene anion– π interactions³³ could reduce halide ion migration, increasing the stability under device operating conditions.⁵ Therefore, supramolecular π -assemblies of arenes and fluoroarenes could be used to control the properties of hybrid perovskites and their composites, although they remain underexploited in this context.

Here, we use NMR crystallography in combination with molecular dynamics (MD) simulations, density functional theory (DFT), and X-ray diffraction to elucidate the atomic-level structure of the spacer cations in a model system that consists of PEA⁺ and/or FEA⁺ spacers (S⁺) in a typical layered 2D perovskite of S₂PbI₄ ($n = 1$) composition. Contrary to previous reports, we reveal that the arene–fluoroarene interactions of the systems studied here do not lead to

templating of a uniform alternating structure, but instead the spacer layers form nanoscale phase-segregated domains. Furthermore, we find that this nanoscale supramolecular structure with mixed-spacers enhances the performance of perovskite solar cells as compared to either of the components alone, which is accompanied by enhanced operational stability. We suggest that nanoscale segregation provides a new route for the design of layered hybrid perovskite systems. This new understanding is provided by the capacity of NMR crystallography to determine the atomic-level structure of the materials, which thus enables rational structure–activity-based design strategies applicable to other hybrid materials.

RESULTS AND DISCUSSION

Hybrid Perovskite Thin Films. This study focuses on the $n = 1$ model system with PEA⁺ and/or FEA⁺ spacers (S⁺) in a S₂PbI₄ layered 2D perovskite composition. Higher compositional representatives of Ruddlesden–Popper S₂A_{n-1}M_nX_{3n+1} systems ($n > 1$) commonly form mixtures of phases (known as quasi-2D perovskites) and are thus not well-defined.^{6,11} Moreover, we assessed 2D/3D composites with overlayers of the organic spacer(s) on the 3D perovskite, which form a thin layer of a 2D phase upon annealing and are relevant for photovoltaic applications.^{12,34} For these materials, we have based our investigation on compositions comprising FA⁺ as the central A⁺ cation due to its higher thermal stability.^{35,36}

Thin films of layered perovskites were prepared based on $n = 1$ S₂PbI₄ compositions (S⁺ = PEA⁺, FEA⁺, and 1:1 PEA⁺:FEA⁺ denoted PF) as well as 3D (Cs_{0.05}FA_{0.95}MA_{0.1})-(PbI₃)_{1.05} perovskite thin films with a spacer overlayer of PEAI, FEAI or 1:1 PEAI:FEAI to form 2D/3D perovskite compositions on the surface, in accordance with the previous reports.³⁴

The structural properties of the resulting perovskite films were analyzed by X-ray diffraction (XRD) in the Bragg–Brentano configuration. XRD patterns of S₂PbI₄ compositions evidence the capacity of all of the spacers to form well-defined layered perovskite structures (Figure 2a). This is revealed by the presence of characteristic periodic patterns and low-angle reflections in the 2θ region below 10° that are associated with the basal ($h00$) planes.⁶ The (FEA)₂PbI₄ films also show

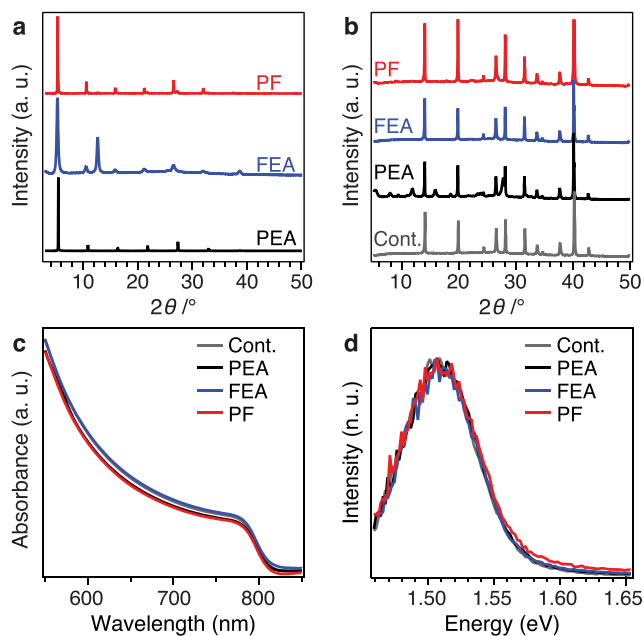


Figure 2. Structural and optical properties of the perovskite thin films. XRD patterns of (a) layered 2D perovskite films of S_2PbI_4 composition and (b) 2D/3D perovskites ($S^+ = PEA^+$, FEA^+ , and 1:1 $PEA^+ : FEA^+$ denoted PF) on glass microscope slides. (c) UV-vis absorption spectra and (d) steady-state PL spectra of 2D/3D perovskite films on microscopic glass slide. n.u. = normalized units; cont. = control.

additional reflections (e.g., around 2θ of 12.6°) that are associated with residual PbI_2 .

For the 2D/3D perovskites (Figure 2b), the overlayers of organic spacers do not substantially change the crystal structure of the 3D perovskite, as the characteristic signals remain unaltered. The PEA-based system features additional low-angle reflections in the region of 2θ below 10° , which are indicative of the formation of low-dimensional perovskite phases.⁶ These signals were not apparent for FEA- and PF-treated perovskite thin films. The low-angle signals could be seen, however, for both the PEA^+ and FEA^+ treated samples using grazing-incidence wide-angle X-ray scattering (GI-WAXS) and X-ray reflectivity (Figure S5). The assemblies of the FEA^+ and PF spacers on the 3D perovskite surface were also probed by X-ray photoelectron spectroscopy (XPS), which confirms the presence of FEA^+ on the surface of the hybrid perovskite through the appearance of F 1s core level signals (Figure S6 shows XPS data for control and treated samples). The F 1s binding energies for FEA- and PF-treated samples of 686.89 and 688.09 eV, respectively, indicate that the organic moieties engage in different binding modes on the surface of the hybrid perovskite. However, the spacer layers were not found to significantly alter the optical properties of the 3D perovskite, as demonstrated by the UV-vis absorption and photoluminescence (PL) spectroscopy of the corresponding films (Figure 2c,d). This is beneficial for maintaining favorable optoelectronic features relevant to their application.

In summary, the analysis of perovskite films of S_2PbI_4 ($n = 1$) composition indicates that the spacer moieties (PEA^+ , FEA^+ , and their 1:1 mixture, PF) form layered 2D perovskite structures. Moreover, the presence of the spacer overlayer does not substantially affect the optoelectronic properties of the resulting 2D/3D perovskite films, which is beneficial for their

application. Although XRD determines the layered 2D nature of the inorganic lattice, it is not sensitive to the structure of the organic spacer cation. The atomic-level structure was therefore investigated by solid-state NMR spectroscopy^{25,37–39} in conjunction with MD simulations and DFT calculations.

Elucidating the Supramolecular Structure. To analyze the bulk properties of the materials, powders of S_2PbI_4 composition ($n = 1$; $S^+ = PEA^+$, FEA^+ , and PF) were prepared mechanochemically.¹⁹ XRD reveals that the crystalline low-dimensional perovskite structure is formed for all compositions, exemplified by the low-angle reflections at around $2\theta = 5.2^\circ$ (Figure 3). These correspond to layer spacings of 16.5, 17.5, and 16.7 Å for $(PEA)_2PbI_4$, $(FEA)_2PbI_4$, and $(PF)_2PbI_4$, respectively, consistent with the trend observed for calculated structures (Figure S3). Many more reflections are seen than for the thin-film samples, due to the lack of preferred orientation. The pattern for $(PEA)_2PbI_4$ is in good agreement with the previously reported crystal structure,⁴⁰ and similar patterns are observed for the other samples. The reflections at 2θ values of ~ 14 – 15° are consistent with in-plane Pb–Pb distances of ~ 6.1 Å. The $(FEA)_2PbI_4$ and $(PF)_2PbI_4$ samples show an additional reflection at 2θ of 12.6° which is ascribed to unreacted PbI_2 , as also observed for the thin-film $(FEA)_2PbI_4$ sample.

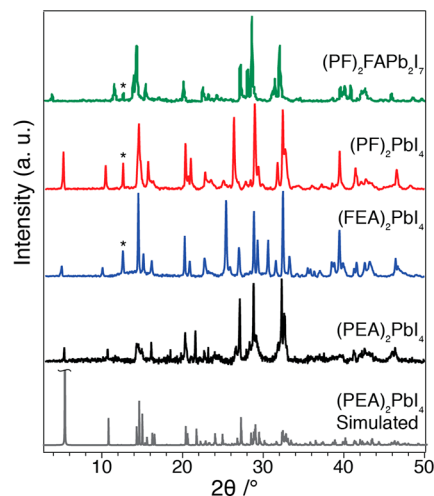


Figure 3. PXRD patterns of mechanothesized layered hybrid perovskites of $S_2FA_{n-1}Pb_nI_4$ composition ($S^+ = PEA^+$, FEA^+ and 1:1 $PEA^+ : FEA^+$ denoted PF). The simulated pattern for $(PEA)_2PbI_4$ is shown for the previously reported (*twisted*) crystal structure.⁴⁰ The major PbI_2 reflection is marked with an asterisk.

Comparison of the $^1H/^{19}F \rightarrow ^{13}C$ cross-polarization (CP) and direct ^{19}F NMR spectra in the aromatic regions of the spacer cations for the pure PEAI and FEAI precursors and for the layered 2D perovskites (Figure 4) shows that the spacer environment changes upon formation of layered 2D perovskites. The ^{19}F spectra for pentafluorophenyl derivatives are well-known.⁴¹ The assignment of the ^{13}C signals for FEAI was determined by $^{19}F \rightarrow ^{13}C$ heteronuclear correlation (HETCOR) spectroscopy (Figure S8), whereas the assignment of the ^{13}C signals for PEA^+ was found by comparison with the calculated shifts, *vide infra*. Ball-milling a 1:1 mixture of PEAI and FEAI under comparable conditions to the mechanochemical preparation of the layered perovskite systems causes only relatively minor changes to the NMR spectra (Figure 4, red spectra, bottom panels). This indicates that the sample adopts

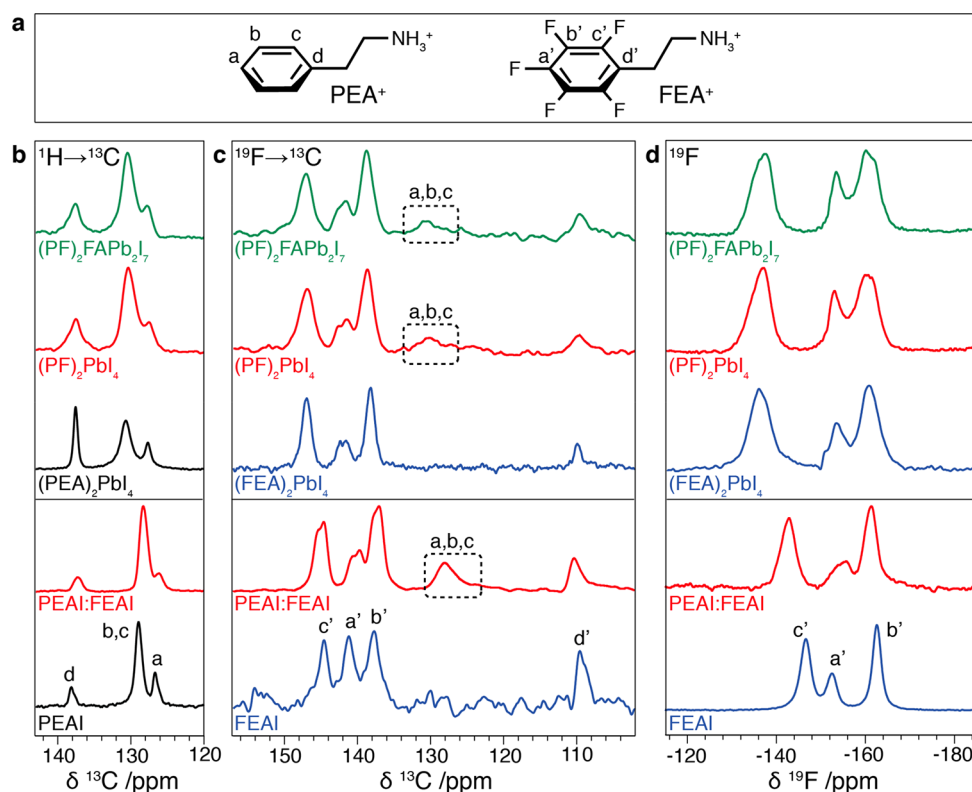


Figure 4. Solid-state NMR spectra of the spacer cations. (a) Structure of PEA⁺ and FEA⁺ cations with the corresponding ¹³C and ¹⁹F sites labeled. (b) ¹H→¹³C CP, (c) ¹⁹F→¹³C CP, and (d) direct ¹⁹F MAS NMR spectra. The top half of the panels are spectra from the layered hybrid perovskites, whereas the bottom half are from the neat spacer salts and their 1:1 mixture, following ball-milling. PF = 1:1 PEA⁺:FEA⁺. Signals arising from PEA⁺ in the ¹⁹F→¹³C CP spectra are highlighted in dashed boxes. Experimental parameters are given in Table S1. Full ¹³C spectra are shown in Figure S7.

a similar structure to the neat spacer precursors. The atomic-level mixing between the phenyl moieties of the two components in the PEAI:FEAI sample is nevertheless clearly evidenced by the signal arising from the PEA⁺ carbons (labeled a–c, Figure 4a) in the ¹⁹F→¹³C CP spectrum (Figure 4c, dashed box). The ¹⁹F spectrum for PEAI:FEAI (Figure 4d) exhibits slightly different shifts compared to pure FEAI, due to the sensitivity of the ¹⁹F shifts to the modified structure. For the layered perovskites, clear differences are observed in the NMR spectra of the spacer cations, implying the formation of a new supramolecular structure (Figure 4b–d, top panels). The spectra for (PF)₂PbI₄ (*n* = 1) and (PF)₂FAPb₂I₇ (*n* = 2) compositions are comparable, which implies that the organic structures are also very similar. This is expected, since the presence of a second layer of lead iodide octahedra should not significantly influence the spacer cations. Furthermore, for both systems, the PEA⁺ carbons can be observed in the ¹⁹F→¹³C CP spectra (Figure 4c, dashed boxes), indicating atomic-scale mixing of the spacer cations, since CP transfer relies on through-space dipole–dipole interactions at the subnanometer length scale. However, the layered perovskites containing only a single type of spacer cation, namely (PEA)₂PbI₄ and (FEA)₂PbI₄, exhibit very similar spectra to the samples with mixed spacers. These observations can be explained by nanoscale segregation due to self-recognition or “narcissistic” self-sorting,⁴² which would result in the local environments remaining similar to the individual spacer structures, while still affording the atomic-level contact observed by ¹⁹F→¹³C CP. The broader signals in the mixed samples may thus correspond to the broader distribution of slightly different possible local

environments experienced within nanodomains of the different spacer cations.

To test whether the results obtained for the bulk mechanosynthesized samples are also applicable to solution-processed thin films, the ¹H→¹³C spectrum was recorded for a thin-film sample of (PF)₂PbI₄ after scraping off the substrate (Figure S7, top). Although the signal-to-noise ratio is relatively low due to the low sample mass, the aromatic signals for the spacer cations are observed with the same shifts as for the bulk (PF)₂PbI₄ sample, within a root-mean-squared error (RMSE) of 0.45 ppm. This indicates that the same supramolecular structure is adopted here for both the bulk and thin-film layered perovskites.

To illuminate the atomic-level structure using the NMR data, the predicted chemical shieldings were calculated using DFT for different trial structures. These were then converted to chemical shifts using a regression obtained from a set of reference organic structures containing fluorine and iodine (for details refer to Sections S3–S5). The *n* = 1 structure was used for the comparison, since the structure of the organic layer is shared by higher order 2D/3D homologues. Trial structures were generated by selecting low-energy structures from molecular dynamics simulations (detailed in Section S3), some of which were based on previously reported crystal structures,^{9,40,43,44} prior to geometry optimization using DFT. Structures with two different relative orientations of the spacer cation aromatic rings were considered: the “twisted” structure (Figure 5a), with a twist between the aromatic rings in the two opposing layers, resulting in predominantly π_T interactions (Figure 1c) and the “parallel” structure (Figure 5b), with

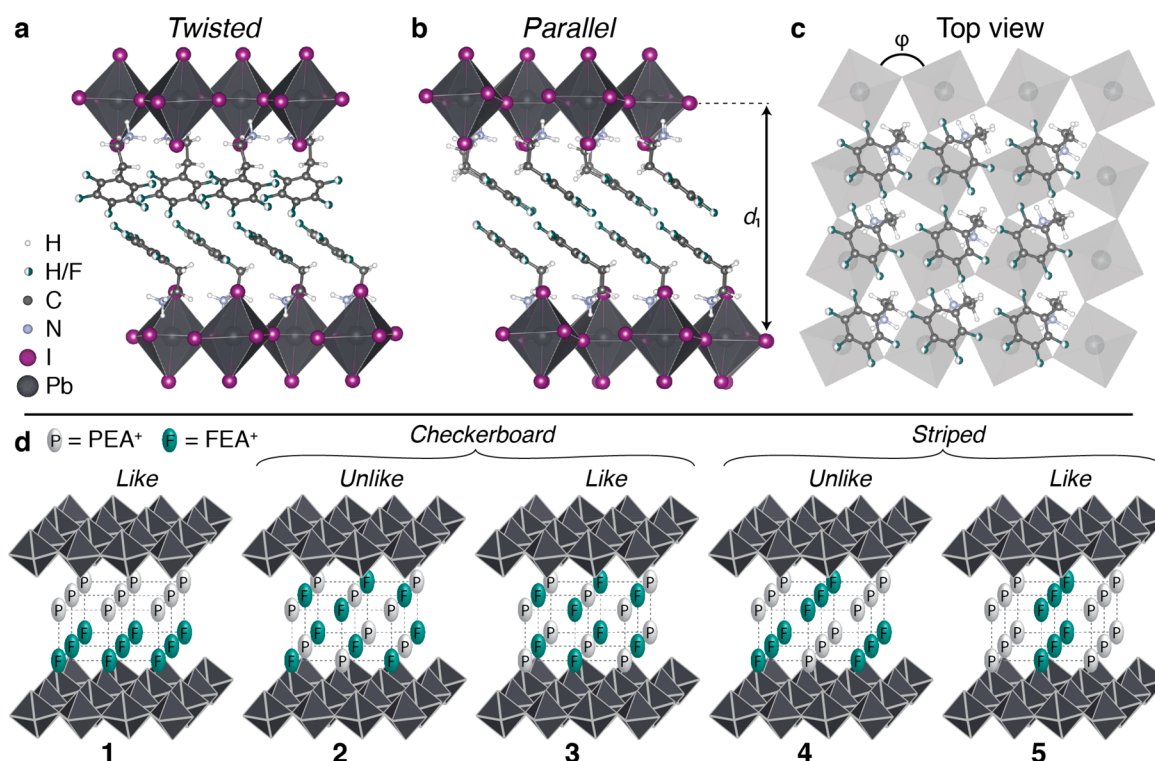


Figure 5. Trial structures for DFT calculations and NMR crystallography of S_2PbI_4 layered perovskites. (a, b) *Twisted* and *parallel* relative orientations of the aromatic rings in adjacent layers and (c) top view of the spacer layer, showing the square lattice of interstices in the inorganic layer. The interlayer spacing (d_i) and octahedral tilting (φ) are also indicated. (d) Schematic of different possible arrangements (1–5) of PEA^+ (P) and FEA^+ (F) moieties on the two opposing lattices representing the spacer bilayer within the layered perovskite.

aromatic rings from opposite layers aligned in parallel planes at 180° between the layers, allowing displaced parallel π_D interactions (Figure 1c). For $(PEA)_2PbI_4$, the experimental ^{13}C shifts agree with the calculated shifts for the *twisted* structure better than for the *parallel* structure (Table S4). This observation is in agreement with the previously reported single crystal structure (CCDC no. 1542461)⁴⁰ and the slightly lower calculated DFT energy (Section S3). For this analysis, only the aromatic carbons in the spacer cations were considered because the aliphatic carbons are close to the heavy Pb and I atoms and may require full relativistic treatment to obtain accurate shieldings. In contrast, for $(FEA)_2PbI_4$, the calculated ^{13}C and ^{19}F shifts for the *parallel* structure are in better agreement with experiment (Table S4), in accordance with the fact that the DFT energy is lower for the *parallel* structure (Section S3).

For the mixed $(PF)_2PbI_4$ layered perovskite, there are many possible arrangements of the PEA^+ and FEA^+ spacers. Each lead iodide layer contains an array of tilted corner-sharing octahedra, resulting in a square lattice of rhombic interstices on each face in which the spacer cations reside (Figure 5c). We have considered the simplest representative examples of tiling the spacer cations over the two opposing lattices to form five trial structures (1–5, Figure 5d). In structure 1, each face comprises only a single type of spacer, while structures 2 and 3 have “checkerboard” arrangements of the cations on each face. In structure 2, the arrangements are offset so that *unlike* spacers are opposite each other (i.e., PEA^+ is opposite FEA^+), while structure 3 has *like* spacers opposing. Finally, structures 4 and 5 have *striped* arrangements of the spacers on each face with *unlike*- and *like*-pairing arrangements of the opposing spacers, respectively. In addition, we also consider a segregated

model, where the shifts are calculated for the separate pure *twisted* $(PEA)_2PbI_4$ and *parallel* $(FEA)_2PbI_4$ structures, to imitate the environments in a nanoscale segregated structure that would form as a result of predominantly narcissistic self-sorting.

Figure 6 compares the experimental and calculated ^{13}C and ^{19}F chemical shifts for the five mixed $(PF)_2PbI_4$ structures and the segregated model with the shifts from the pure $(PEA)_2PbI_4$ and $(FEA)_2PbI_4$ structures. The best agreement was found for a segregated model, and this is the only case for which the RMSEs between the calculated and experimental chemical shifts (Figure 6, insets) are less than the expected RMSE in DFT calculated shifts: 2.32 and 1.98 ppm for ^{13}C and ^{19}F , respectively, as estimated by the error in the calculated shifts for the external reference set (Section S5.2). Bayesian analysis of the data with the Bayesian NMR tool⁴⁵ indicates that the segregated system matches the experimental data with 99.9% probability, which is also consistent with the experimental shifts for $(PF)_2PbI_4$ being very similar to those for $(PEA)_2PbI_4$ and $(FEA)_2PbI_4$.

We therefore conclude that the layered hybrid perovskite structure formed by mixed PEA^+ and FEA^+ spacers comprises segregated domains of the two spacer moieties; however, since the PEA^+ ^{13}C signals are observed in the $^{19}F \rightarrow ^{13}C$ CP spectrum (Figure 4c), the domains must be limited to the nanoscale. Although the opposite quadrupolar moments of the aromatic systems were expected to favor $PEA^+ - FEA^+$ π interactions, the segregation may reflect the differing preferences of the two spacer cations to form *twisted* and *parallel* aromatic contacts, respectively (Figure 5a,b). Nevertheless, nanoscale mixing of the two spacers is observed, which may be entropically driven and is further supported by the

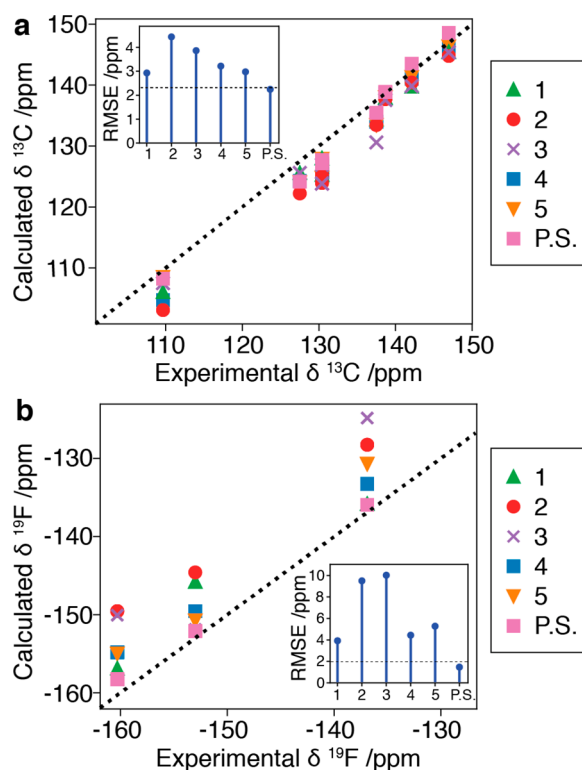


Figure 6. NMR shift calculations. Calculated aromatic (a) ^{13}C and (b) ^{19}F chemical shifts plotted against the experimental $(\text{PF})_2\text{PbI}_4$ chemical shifts for structures 1–5 (Figure Sd) and a phase segregated model (P.S., the calculated shifts for pure $(\text{PEA})_2\text{PbI}_4$ and $(\text{FEA})_2\text{PbI}_4$). The dashed diagonal lines indicate exact agreement. The insets show the RMSE between the calculated and experimental chemical shifts for each structure, and the horizontal lines are the expected error in DFT calculated shifts given by the RMSE in the regression set.

single basal reflection observed by XRD (Figure 3), despite the pure layered 2D perovskites having different layer spacings (*vide supra*). As a result, the photovoltaic performance of the mixed system could be affected as compared to the pure system (*vide infra*) through a synergistic effect

Photovoltaic Performance and Stability. The photovoltaic performance of hybrid perovskites with overlayers of layered perovskites with the different spacer cations was investigated using devices with the conventional fluorine-doped tin oxide (FTO)/*c*-TiO₂ (40 nm)/ mp-TiO₂ (250 nm)/ perovskite (450 nm)/2,2',7,7'-tetrakis(*N,N*-di-4-methoxyphenylamino)-9,9'-spirobifluorene (Spiro-OMeTAD; 180 nm)/Au (80 nm) configuration to probe their utility (Figure 7a–d). The layer thicknesses were estimated by cross-sectional SEM imaging (Figure 7c and Figure S9), and the photovoltaic (PV) metrics were extracted from the current–voltage (*J*–*V*) characteristics (Figure 7a,d and Figure S10). The differences between the short-circuit currents (*J*_{SC}) for different compositions were found to be rather small, in the range of approximately 1%. This is in accordance with the minor changes in the optoelectronic properties of the 2D/3D perovskite films (Figure 2c,d). DFT-calculated band gaps of S₂PbI₄ systems (S⁺ = PEA⁺, FEA⁺, and PF; Figure S1) revealed that nonfluorinated systems have lower gaps, which coincides with their less pronounced octahedral tilting compared to the fluorinated systems (Figure S2) as well as lower interlayer distances (Figure S3). The current density obtained by

integrating the incident photon-to-current efficiency (IPCE) as a function of wavelength for the champion device, 24.4 mA cm^{−2}, is in good agreement with the values obtained from the *J*–*V* data (24.8 mA cm^{−2}), excluding any mismatch between the simulator and AM 1.5G light source (Figure 7b and Figure S11). Unlike the *J*_{SC}, the open-circuit voltages (*V*_{OC}) of treated devices increased on average for PEA⁺ and PF systems by 30 mV and 45 mV, respectively, which is likely to be associated with the role of the spacer overlayer in passivating the surface defects. The improvement in *V*_{OC} resulting from a low-dimensional overlayer is in agreement with numerous previous studies.^{25,46,47} However, while the fill factor (FF) of FEA⁺-treated devices decreased relative to the controls, it increased for PF-treated devices. As a result, the mean PCEs of control, PEA⁺, FEA⁺, and PF-treated devices were 19.6%, 19.6%, 18.7%, and 20.8%, respectively, with the champion device reaching an efficiency of 21.6% for the PF-treated system (Figure 7a and Figure S10).

Notably, the performance of the mixed-spacer treated device, which we have determined to have a nanoscale-segregated structure of the spacer cations, shows a higher power conversion efficiency than with either spacer individually. We note, however, that the photovoltaic performances were not the primary objective of this study and were instead analyzed to illustrate the utility of this class of hybrid perovskites; therefore, further optimization of the corresponding devices can be envisaged. We further examined the effect of the overlayer on the operational stability of unencapsulated devices by monitoring the evolution of their maximum power point (MPP) under continuous irradiation of 1 sun in a nitrogen atmosphere (Figure 7e), which has previously been found to play a role in suppressing the degradation under operational conditions.^{48,49} While the initial performance of the control devices dropped to values below 80% after just 20 h of operation, the treated devices showed improved stability during this period of time, maintaining around 90% of their initial performance value after 100 h of operation. These performance and stability improvements indicate the potential of such mixed-spacer layered perovskites in perovskite photovoltaics, which should stimulate further investigations.

CONCLUSION

In summary, we present a systematic NMR crystallography approach based on solid-state NMR spectroscopy and computational analysis to elucidate the supramolecular structure of the organic spacer layer for layered hybrid perovskites. Specifically, a mixed arene–fluoroarene model system was studied, for which we find that although there is atomic-level contact between the spacers, the structures most closely resemble those of the end-members, implying nanoscale segregation. We illustrate the application of this system in enhancing the performance and stability of perovskite solar cells and demonstrate that the performance is greater than for either of the spacers individually. In general, we envisage that NMR crystallography will play an important role in determining the supramolecular structure of layered hybrid perovskites, facilitating molecular design of spacer systems driven by an understanding of their assemblies, thereby advancing the properties and applications of hybrid materials.

EXPERIMENTAL SECTION

Layered perovskite thin films were deposited on microscope glass slides from a 0.5 M precursor solution by spin-coating, followed by

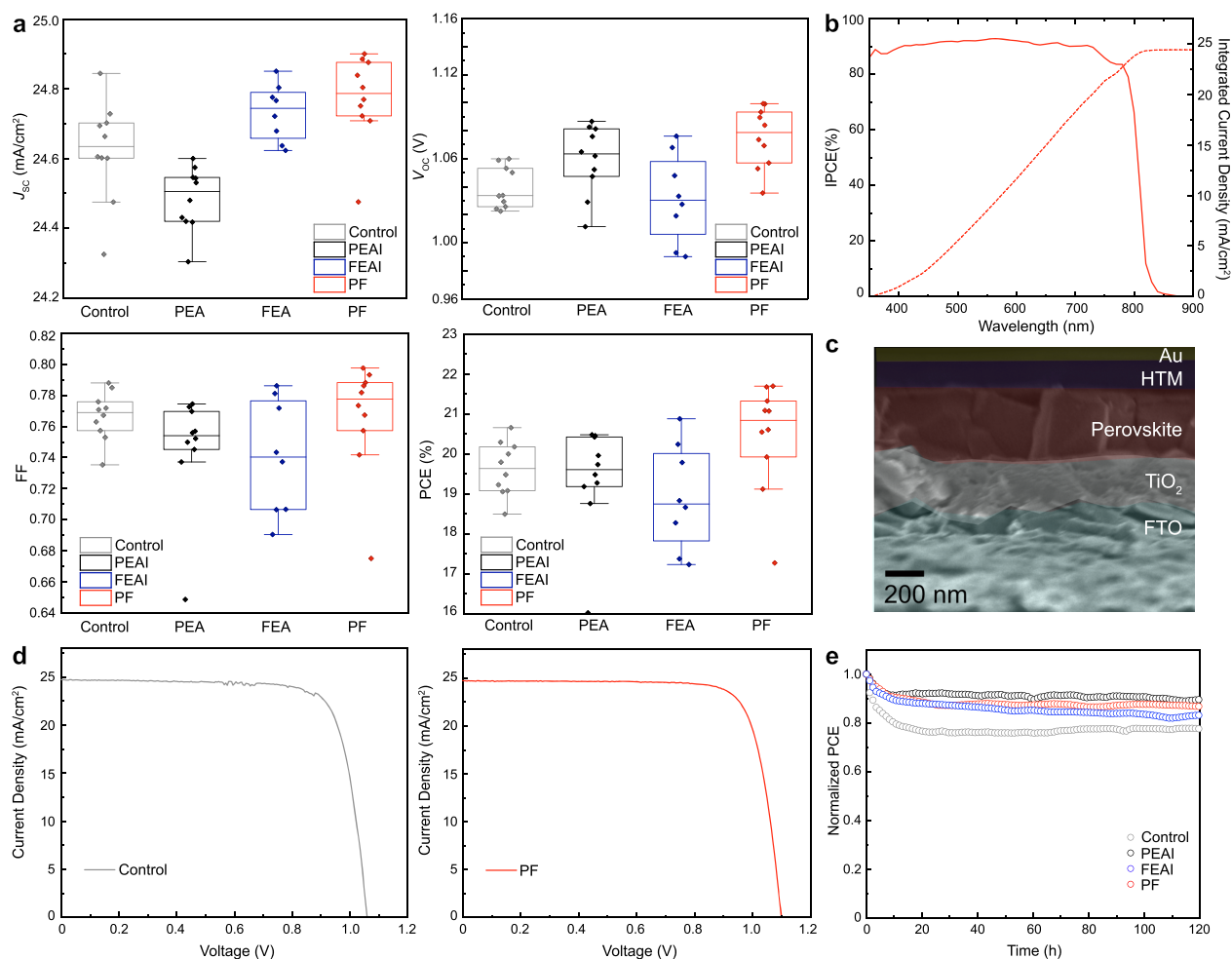


Figure 7. Photovoltaic performance and operational stability. (a) PV metrics of representative control and treated devices with aperture areas of 0.16 cm² under full solar intensity at ambient temperature in reverse (from V_{oc} to J_{sc}) and forward bias with the PV metrics. $J-V$ curves were recorded at a scanning rate of 50 mV s⁻¹ under standard AM 1.5G solar radiation. (b) IPCE spectrum of the champion device with the projected photocurrent derived by integrating the IPCE over the spectral emission. (c) Cross-sectional SEM image of the photovoltaic device of FTO/cp-TiO₂/mp-TiO₂/perovskite/Spiro-OMeTAD/Au architecture. (d) $J-V$ curves of champion control (left) and PF-treated (right) devices. (e) Evolution of the MPP over time upon 1 sun illumination in nitrogen atmosphere at 60 °C.

annealing at 120 °C for 15 min. 2D/3D thin films were similarly prepared by spin-coating with a 1.5 M perovskite precursor solution, followed by annealing at 120 °C for 10 min and 100 °C for 40 min, before spin-coating an overlayer with a 30 mM solution of the spacer precursor in isopropanol at ambient temperature, followed by annealing at 110 °C for 5 min. Full details are provided in Section S1. Details on device characterization are given in Section S2.

Bulk layered perovskite powders were prepared by mechano-synthesis according to previous protocols.^{38,50}

Solid-state NMR spectra were recorded at 9.4, 11.7, or 21.1 T. Full details are given in Section S2 and Table S1. Samples were annealed at 150 °C before recording the NMR.

Trial structures for the layered perovskites were determined from MD simulations and DFT calculations following an analogous procedure as previously reported.⁵¹ Details are provided in Section S3 and S4.

NMR crystallography was used to determine the structure of the organic spacers, and the chemical shifts were calculated for the different trial structures using DFT (Section S5).

■ ASSOCIATED CONTENT

SI Supporting Information

The Supporting Information is available free of charge at <https://pubs.acs.org/doi/10.1021/jacs.0c11563>.

Experimental details for device preparation, synthesis, characterization, solid-state NMR, MD and DFT calculations as well as supplementary data (PDF)

The raw data for this work (including NMR data, molecular dynamics data, structure files, photovoltaic data, and additional characterization data) are deposited at DOI: 10.5281/zenodo.4427776

■ AUTHOR INFORMATION

Corresponding Authors

Lyndon Emsley – Laboratory of Magnetic Resonance, École Polytechnique Fédérale de Lausanne, Lausanne CH-1015, Switzerland; orcid.org/0000-0003-1360-2572; Email: lyndon.emsley@epfl.ch

Jovana V. Milić – Laboratory of Photonics and Interfaces, École Polytechnique Fédérale de Lausanne, Lausanne CH-1015, Switzerland; orcid.org/0000-0002-9965-3460; Email: jovana.milic@epfl.ch

Michael Grätzel – Laboratory of Photonics and Interfaces, École Polytechnique Fédérale de Lausanne, Lausanne CH-1015, Switzerland; orcid.org/0000-0002-0068-0195; Email: michael.gratzel@epfl.ch

Ursula Rothlisberger – Laboratory of Computational Chemistry and Biochemistry, École Polytechnique Fédérale de Lausanne, Lausanne CH-1015, Switzerland; orcid.org/0000-0002-1704-8591; Email: ursula.rothlisberger@epfl.ch

Authors

Michael A. Hope – Laboratory of Magnetic Resonance, École Polytechnique Fédérale de Lausanne, Lausanne CH-1015, Switzerland; orcid.org/0000-0002-4742-9336

Toru Nakamura – Laboratory of Photonics and Interfaces, École Polytechnique Fédérale de Lausanne, Lausanne CH-1015, Switzerland; Technology Innovation Division, Panasonic Corporation, Osaka 570-8501, Japan; orcid.org/0000-0002-4290-4695

Paramvir Ahlawat – Laboratory of Computational Chemistry and Biochemistry, École Polytechnique Fédérale de Lausanne, Lausanne CH-1015, Switzerland; orcid.org/0000-0003-2355-3663

Aditya Mishra – Laboratory of Magnetic Resonance, École Polytechnique Fédérale de Lausanne, Lausanne CH-1015, Switzerland

Manuel Cordova – Laboratory of Magnetic Resonance, École Polytechnique Fédérale de Lausanne, Lausanne CH-1015, Switzerland; orcid.org/0000-0002-8722-6541

Farzaneh Jahanbakhshi – Laboratory of Computational Chemistry and Biochemistry, École Polytechnique Fédérale de Lausanne, Lausanne CH-1015, Switzerland; orcid.org/0000-0001-7113-2746

◆ **Marko Mladenović** – Laboratory of Computational Chemistry and Biochemistry, École Polytechnique Fédérale de Lausanne, Lausanne CH-1015, Switzerland

Rashmi Runjhun – Laboratory of Photonics and Interfaces, École Polytechnique Fédérale de Lausanne, Lausanne CH-1015, Switzerland; Institute of Physical Chemistry, Polish Academy of Sciences, Warsaw 01-224, Poland

Lena Merten – Institut für Angewandte Physik, Universität Tübingen, 72076 Tübingen, Germany

Alexander Hinderhofer – Institut für Angewandte Physik, Universität Tübingen, 72076 Tübingen, Germany; orcid.org/0000-0001-8152-6386

Brian I. Carlsen – Laboratory of Photomolecular Science, École Polytechnique Fédérale de Lausanne, Lausanne CH-1015, Switzerland

¶ **Dominik J. Kubicki** – Laboratory of Magnetic Resonance, École Polytechnique Fédérale de Lausanne, Lausanne CH-1015, Switzerland; orcid.org/0000-0002-9231-6779

Renana Gershoni-Poranne – Laboratory of Chemistry and Applied Biosciences, ETH Zurich, 8092 Zurich, Switzerland; orcid.org/0000-0002-2233-6854

Thomas Schneeberger – Laboratory of Photonics and Interfaces, École Polytechnique Fédérale de Lausanne, Lausanne CH-1015, Switzerland

Loïc C. Carbone – Laboratory of Photonics and Interfaces, École Polytechnique Fédérale de Lausanne, Lausanne CH-1015, Switzerland

Yuhang Liu – Laboratory of Photonics and Interfaces, École Polytechnique Fédérale de Lausanne, Lausanne CH-1015, Switzerland

Shaik M. Zakeeruddin – Laboratory of Photonics and Interfaces, École Polytechnique Fédérale de Lausanne, Lausanne CH-1015, Switzerland

Janusz Lewinski – Institute of Physical Chemistry, Polish Academy of Sciences, Warsaw 01-224, Poland; orcid.org/0000-0002-3407-0395

Anders Hagfeldt – Laboratory of Photomolecular Science, École Polytechnique Fédérale de Lausanne, Lausanne CH-1015, Switzerland; orcid.org/0000-0001-6725-8856

Frank Schreiber – Institut für Angewandte Physik, Universität Tübingen, 72076 Tübingen, Germany

Complete contact information is available at: <https://pubs.acs.org/10.1021/jacs.0c11563>

Author Contributions

◇ These authors contributed equally.

Notes

The authors declare no competing financial interest.

¶ Cavendish Laboratory, University of Cambridge, United Kingdom CB3 0HE

◆ Scientific Computing Laboratory, Center for the Study of Complex Systems, Institute of Physics Belgrade, University of Belgrade, Pregrevica 118, 11080 Belgrade, Serbia

● Soft Matter Physics Group at the Adolphe Merkle Institute of the University of Fribourg, 1700 Fribourg, Switzerland.

ACKNOWLEDGMENTS

L.E. is grateful for financial support from SNSF grant no. 200020_178860. J.V.M., S.M.Z., and M.G. are grateful to the European Union's Horizon 2020 research and innovation program under grant agreement no. 826013 (IMPRESSIVE). J.V.M. acknowledges support from the Swiss National Science Foundation (SNSF) grant no. 193174. U.R. acknowledges SNSF grant no. 200020-165863, NCCR-MUST, NRP70, and the SINERGIA interdisciplinary research program EPISODE for funding. R.R. acknowledges funding from the European Union's Horizon 2020 research and innovation program under the Marie Skłodowska Curie grant agreement no. 711859 and the Polish Ministry of Science and Higher Education from the cofunded project, grant agreement no. 3549/H2020/CO-FUND2016/2. We would like to thank several colleagues at EPFL for their support in the course of this study: Dr. Dan Ren for performing a TEM study, Dr. Linfeng Pan for support with the XRD of the films, Dr. Sandy Sanchez for support with the XRD and SEM of the films, Dr. Claudia Avalos for support in performing NMR experiments, and Masaud Almalki and Anwar Alanazi for preparing supplementary samples of films and devices.

REFERENCES

- (1) Jena, A. K.; Kulkarni, A.; Miyasaka, T. Halide Perovskite Photovoltaics: Background, Status, and Future Prospects. *Chem. Rev.* **2019**, *119*, 3036–3103.
- (2) Kim, H. S.; Lee, C. R.; Im, J. H.; Lee, K. B.; Moehl, T.; Marchioro, A.; Moon, S. J.; Humphry-Baker, R.; Yum, J. H.; Moser, J. E.; Grätzel, M.; Park, N. G. Lead Iodide Perovskite Sensitized All-Solid-State Submicron Thin Film Mesoscopic Solar Cell with Efficiency Exceeding 9%. *Sci. Rep.* **2012**, *2*, 591.
- (3) Eperon, G. E.; Stranks, S. D.; Menelaou, C.; Johnston, M. B.; Herz, L. M.; Snaith, H. J. Formamidinium Lead Trihalide: A Broadly Tunable Perovskite for Efficient Planar Heterojunction Solar Cells. *Energy Environ. Sci.* **2014**, *7*, 982–988.
- (4) Grätzel, M. The Rise of Highly Efficient and Stable Perovskite Solar Cells. *Acc. Chem. Res.* **2017**, *50*, 487–491.
- (5) Wang, R.; Mujahid, M.; Duan, Y.; Wang, Z.-K.; Xue, J.; Yang, Y. A Review of Perovskites Solar Cell Stability. *Adv. Funct. Mater.* **2019**, *29*, 1808843.

- (6) Mao, L.; Stoumpos, C. C.; Kanatzidis, M. G. Two-Dimensional Hybrid Halide Perovskites: Principles and Promises. *J. Am. Chem. Soc.* **2019**, *141*, 1171–1190.
- (7) Mao, L.; Ke, W.; Pedesseau, L.; Wu, Y.; Katan, C.; Even, J.; Wasielewski, M. R.; Stoumpos, C. C.; Kanatzidis, M. G. Hybrid Dion–Jacobson 2D Lead Iodide Perovskites. *J. Am. Chem. Soc.* **2018**, *140*, 3775–3783.
- (8) Tsai, H.; Nie, W.; Blancon, J.-C.; Stoumpos, C. C.; Asadpour, R.; Harutyunyan, B.; Neukirch, A. J.; Verduzco, R.; Crochet, J. J.; Tretiak, S.; Pedesseau, L.; Even, J.; Alam, M. A.; Gupta, G.; Lou, J.; Ajayan, P. M.; Bedzyk, M. J.; Kanatzidis, M. G.; Mohite, A. D. High-Efficiency Two-Dimensional Ruddlesden–Popper Perovskite Solar Cells. *Nature* **2016**, *536*, 312–316.
- (9) Smith, I. C.; Hoke, E. T.; Solis-Ibarra, D.; McGehee, M. D.; Karunadasa, H. I. A Layered Hybrid Perovskite Solar Cell Absorber with Enhanced Moisture Stability. *Angew. Chem., Int. Ed.* **2014**, *53*, 11232–11235.
- (10) Grancini, G.; Nazeeruddin, M. K. Dimensional Tailoring of Hybrid Perovskites for Photovoltaics. *Nat. Rev. Mater.* **2019**, *4*, 4–22.
- (11) Saparov, B.; Mitzi, D. B. Organic–Inorganic Perovskites: Structural Versatility for Functional Materials Design. *Chem. Rev.* **2016**, *116*, 4558–4596.
- (12) Grancini, G.; Roldán-Carmona, C.; Zimmermann, I.; Mosconi, E.; Lee, X.; Martineau, D.; Narbey, S.; Oswald, F.; De Angelis, F.; Nazeeruddin, M. K. One-Year Stable Perovskite Solar Cells by 2D/3D Interface Engineering. *Nat. Commun.* **2017**, *8*, 15684.
- (13) Li, X.; Guo, P.; Kepenekian, M.; Hadar, I.; Katan, C.; Even, J.; Stoumpos, C. C.; Schaller, R. D.; Kanatzidis, M. G. Small Cyclic Diammonium Cation Templated (110)-Oriented 2D Halide (X = I, Br, Cl) Perovskites with White-Light Emission. *Chem. Mater.* **2019**, *31*, 3582–3590.
- (14) Alanazi, A. Q.; Kubicki, D. J.; Prochowicz, D.; Alharbi, E. A.; Bouduban, M. E. F.; Jahanbakhshi, F.; Mladenović, M.; Milić, J. V.; Giordano, F.; Ren, D.; Alyamani, A. Y.; Albrithen, H.; Albadi, A.; Alotaibi, M. H.; Moser, J.-E.; Zakeeruddin, S. M.; Rothlisberger, U.; Emsley, L.; Grätzel, M. Atomic-Level Microstructure of Efficient Formamidinium-Based Perovskite Solar Cells Stabilized by 5-Ammonium Valeric Acid Iodide Revealed by Multinuclear and Two-Dimensional Solid-State NMR. *J. Am. Chem. Soc.* **2019**, *141*, 17659–17669.
- (15) Ashari-Astani, N.; Jahanbakhshi, F.; Mladenović, M.; Alanazi, A. Q. M.; Ahmadabadi, I.; Ejtehadi, M. R.; Dar, M. I.; Grätzel, M.; Rothlisberger, U. Ruddlesden Popper Phases of Methylammonium-Based Two-Dimensional Perovskites with 5-Ammonium Valeric Acid $\text{AVA}_2\text{MA}_{n-1}\text{Pb}_n\text{I}_{3n+1}$ with $n = 1, 2$, and 3 . *J. Phys. Chem. Lett.* **2019**, *10*, 3543–3549.
- (16) Jahanbakhshi, F.; Mladenović, M.; Kneschaurek, E.; Merten, L.; Gélvez-Rueda, M. C.; Ahlawat, P.; Li, Y.; Dučinskas, A.; Hinderhofer, A.; Dar, M. I.; Tress, W.; Carlsen, B.; Ummadisingu, A.; Zakeeruddin, S. M.; Hagfeldt, A.; Schreiber, F.; Grozema, F. C.; Rothlisberger, U.; Milić, J. V.; Graetzel, M. Unravelling the Structural Complexity and Photophysical Properties of Adamantyl-Based Layered Hybrid Perovskites. *J. Mater. Chem. A* **2020**, *8*, 17732–17740.
- (17) Bi, D.; Li, X.; Milić, J. V.; Kubicki, D. J.; Pellet, N.; Luo, J.; LaGrange, T.; Mettraux, P.; Emsley, L.; Zakeeruddin, S. M.; Grätzel, M. Multifunctional Molecular Modulators for Perovskite Solar Cells with over 20% Efficiency and High Operational Stability. *Nat. Commun.* **2018**, *9*, 4482.
- (18) Abate, A.; Saliba, M.; Hollman, D. J.; Stranks, S. D.; Wojciechowski, K.; Avolio, R.; Grancini, G.; Petrozza, A.; Snaith, H. J. Supramolecular Halogen Bond Passivation of Organic–Inorganic Halide Perovskite Solar Cells. *Nano Lett.* **2014**, *14*, 3247–3254.
- (19) Ruiz-Preciado, M. A.; Kubicki, D. J.; Hofstetter, A.; McGovern, L.; Futscher, M. H.; Ummadisingu, A.; Gershoni-Poranne, R.; Zakeeruddin, S. M.; Ehrler, B.; Emsley, L.; Milić, J. V.; Grätzel, M. Supramolecular Modulation of Hybrid Perovskite Solar Cells via Bifunctional Halogen Bonding Revealed by Two-Dimensional ^{19}F Solid-State NMR Spectroscopy. *J. Am. Chem. Soc.* **2020**, *142*, 1645–1654.
- (20) Mitzi, D. B.; Medeiros, D. R.; Malenfant, P. R. L. Intercalated Organic–Inorganic Perovskites Stabilized by Fluoroaryl–Aryl Interactions. *Inorg. Chem.* **2002**, *41*, 2134–2145.
- (21) Hu, J.; Oswald, I. W. H.; Hu, H.; Stuard, S. J.; Nahid, M. M.; Yan, L.; Chen, Z.; Ade, H.; Neilson, J. R.; You, W. Aryl-Perfluoroaryl Interaction in Two-Dimensional Organic–Inorganic Hybrid Perovskites Boosts Stability and Photovoltaic Efficiency. *ACS Mater. Lett.* **2019**, *1*, 171–176.
- (22) Li, Y.; Milić, J. V.; Ummadisingu, A.; Seo, J.-Y.; Im, J.-H.; Kim, H.-S.; Liu, Y.; Dar, M. I.; Zakeeruddin, S. M.; Wang, P.; Hagfeldt, A.; Grätzel, M. Bifunctional Organic Spacers for Formamidinium-Based Hybrid Dion–Jacobson Two-Dimensional Perovskite Solar Cells. *Nano Lett.* **2019**, *19*, 150–157.
- (23) Gélvez-Rueda, M. C.; Ahlawat, P.; Merten, L.; Jahanbakhshi, F.; Mladenović, M.; Hinderhofer, A.; Dar, M. I.; Li, Y.; Dučinskas, A.; Carlsen, B.; Tress, W.; Ummadisingu, A.; Zakeeruddin, S. M.; Schreiber, F.; Hagfeldt, A.; Rothlisberger, U.; Grozema, F. C.; Milić, J. V.; Graetzel, M. Formamidinium-Based Dion–Jacobson Layered Hybrid Perovskites: Structural Complexity and Optoelectronic Properties. *Adv. Funct. Mater.* **2020**, *30*, 2003428.
- (24) Zhang, J.; Wang, Z.; Mishra, A.; Yu, M.; Shasti, M.; Tress, W.; Kubicki, D. J.; Avalos, C. E.; Lu, H.; Liu, Y.; Carlsen, B. I.; Agarwalla, A.; Wang, Z.; Xiang, W.; Emsley, L.; Zhang, Z.; Grätzel, M.; Guo, W.; Hagfeldt, A. Intermediate Phase Enhances Inorganic Perovskite and Metal Oxide Interface for Efficient Photovoltaics. *Joule* **2020**, *4*, 222–234.
- (25) Alharbi, E. A.; Alyamani, A. Y.; Kubicki, D. J.; Uhl, A. R.; Walder, B. J.; Alanazi, A. Q.; Luo, J.; Burgos-Caminal, A.; Albadi, A.; Albrithen, H.; Alotaibi, M. H.; Moser, J.-E.; Zakeeruddin, S. M.; Giordano, F.; Emsley, L.; Grätzel, M. Atomic-Level Passivation Mechanism of Ammonium Salts Enabling Highly Efficient Perovskite Solar Cells. *Nat. Commun.* **2019**, *10*, 3008.
- (26) Karmakar, A.; Dodd, M. S.; Zhang, X.; Oakley, M. S.; Klobukowski, M.; Michaelis, V. K. Mechanochemical Synthesis of 0D and 3D Cesium Lead Mixed Halide Perovskites. *Chem. Commun.* **2019**, *55*, 5079–5082.
- (27) Franssen, W. M. J.; van Es, S. G. D.; Dervişoğlu, R.; de Wijs, G. A.; Kentgens, A. P. M. Symmetry, Dynamics, and Defects in Methylammonium Lead Halide Perovskites. *J. Phys. Chem. Lett.* **2017**, *8*, 61–66.
- (28) Bryce, D. NMR Crystallography: Structure and Properties of Materials from Solid-State Nuclear Magnetic Resonance Observables. *IUCrJ* **2017**, *4*, 350–359.
- (29) Chen, P.; Bai, Y.; Wang, S.; Lyu, M.; Yun, J.-H.; Wang, L. In Situ Growth of 2D Perovskite Capping Layer for Stable and Efficient Perovskite Solar Cells. *Adv. Funct. Mater.* **2018**, *28*, 1706923.
- (30) Xu, Z.; Mitzi, D. B. SnI_4 -Based Hybrid Perovskites Templated by Multiple Organic Cations: Combining Organic Functionalities through Noncovalent Interactions. *Chem. Mater.* **2003**, *15*, 3632–3637.
- (31) Sutton, C.; Risko, C.; Brédas, J.-L. Noncovalent Intermolecular Interactions in Organic Electronic Materials: Implications for the Molecular Packing vs Electronic Properties of Acenes. *Chem. Mater.* **2016**, *28*, 3–16.
- (32) Kim, K. S.; Tarakeshwar, P.; Lee, J. Y. Molecular Clusters of π -Systems: Theoretical Studies of Structures, Spectra, and Origin of Interaction Energies. *Chem. Rev.* **2000**, *100*, 4145–4186.
- (33) Giese, M.; Albrecht, M.; Rissanen, K. Anion– π Interactions with Fluoroarenes. *Chem. Rev.* **2015**, *115*, 8867–8895.
- (34) Liu, Y.; Akin, S.; Pan, L.; Uchida, R.; Arora, N.; Milić, J. V.; Hinderhofer, A.; Schreiber, F.; Uhl, A. R.; Zakeeruddin, S. M.; Hagfeldt, A.; Dar, M. I.; Grätzel, M. Ultrahydrophobic 3D/2D Fluoroarene Bilayer-Based Water-Resistant Perovskite Solar Cells with Efficiencies Exceeding 22%. *Sci. Adv.* **2019**, *5*, eaaw2543.
- (35) Weller, M. T.; Weber, O. J.; Frost, J. M.; Walsh, A. Cubic Perovskite Structure of Black Formamidinium Lead Iodide, α -[$\text{HC}(\text{NH}_2)_2$]PbI₃, at 298 K. *J. Phys. Chem. Lett.* **2015**, *6*, 3209–3212.

(36) Binek, A.; Hanusch, F. C.; Docampo, P.; Bein, T. Stabilization of the Trigonal High Temperature Phase of Formamidinium Lead Iodide. *J. Phys. Chem. Lett.* **2015**, *6*, 1249–1253.

(37) Franssen, W. M. J.; Kentgens, A. P. M. Solid-state NMR of Hybrid Halide Perovskites. *Solid State Nucl. Magn. Reson.* **2019**, *100*, 36–44.

(38) Kubicki, D. J.; Prochowicz, D.; Hofstetter, A.; Zakeeruddin, S. M.; Grätzel, M.; Emsley, L. Phase Segregation in Cs-, Rb- and K-Doped Mixed-Cation (MA)_x(FA)_{1-x}PbI₃ Hybrid Perovskites from Solid-State NMR. *J. Am. Chem. Soc.* **2017**, *139*, 14173–14180.

(39) Krishna, A.; Akhavan Kazemi, M. A.; Sliwa, M.; Reddy, G. N. M.; Delevoye, L.; Lafon, O.; Felten, A.; Do, M. T.; Gottis, S.; Sauvage, F. Defect Passivation via the Incorporation of Tetrapropylammonium Cation Leading to Stability Enhancement in Lead Halide Perovskite. *Adv. Funct. Mater.* **2020**, *30*, 1909737.

(40) Du, K.-z.; Tu, Q.; Zhang, X.; Han, Q.; Liu, J.; Zauscher, S.; Mitzi, D. B. Two-Dimensional Lead(II) Halide-Based Hybrid Perovskites Templated by Acene Alkylamines: Crystal Structures, Optical Properties, and Piezoelectricity. *Inorg. Chem.* **2017**, *56*, 9291–9302.

(41) Hogben, M. G.; Graham, W. A. G. Chemical Shifts and Coupling Constants in Pentafluorophenyl Derivatives. I. Correlations of Chemical Shifts, Coupling Constants, and π -electronic Interactions. *J. Am. Chem. Soc.* **1969**, *91*, 283–291.

(42) Safont-Sempere, M. M.; Fernandez, G.; Würthner, F. Self-Sorting Phenomena in Complex Supramolecular Systems. *Chem. Rev.* **2011**, *111*, 5784–5814.

(43) Slavney, A. H.; Smaha, R. W.; Smith, I. C.; Jaffe, A.; Umeyama, D.; Karunadasa, H. I. Chemical Approaches to Addressing the Instability and Toxicity of Lead-Halide Perovskite Absorbers. *Inorg. Chem.* **2017**, *56*, 46–55.

(44) Straus, D. B.; Iotov, N.; Gau, M. R.; Zhao, Q.; Carroll, P. J.; Kagan, C. R. Longer Cations Increase Energetic Disorder in Excitonic 2D Hybrid Perovskites. *J. Phys. Chem. Lett.* **2019**, *10*, 1198–1205.

(45) Engel, E. A.; Anelli, A.; Hofstetter, A.; Paruzzo, F.; Emsley, L.; Ceriotti, M. A Bayesian approach to NMR crystal structure determination. *Phys. Chem. Chem. Phys.* **2019**, *21*, 23385–23400.

(46) Chavan, R. D.; Prochowicz, D.; Tavakoli, M. M.; Yadav, P.; Hong, C. K. Surface Treatment of Perovskite Layer with Guanidinium Iodide Leads to Enhanced Moisture Stability and Improved Efficiency of Perovskite Solar Cells. *Adv. Mater. Interfaces* **2020**, *7*, 2000105.

(47) Hu, Y.; Schlipf, J.; Wussler, M.; Petrus, M. L.; Jaegermann, W.; Bein, T.; Müller-Buschbaum, P.; Docampo, P. Hybrid Perovskite/Perovskite Heterojunction Solar Cells. *ACS Nano* **2016**, *10*, 5999–6007.

(48) Domanski, K.; Roose, B.; Matsui, T.; Saliba, M.; Turren-Cruz, S. H.; Correa-Baena, J. P.; Carmona, C. R.; Richardson, G.; Foster, J. M.; De Angelis, F.; Ball, J. M.; Petrozza, A.; Mine, N.; Nazeeruddin, M. K.; Tress, W.; Grätzel, M.; Steiner, U.; Hagfeldt, A.; Abate, A. Migration of Cations Induces Reversible Performance Losses Over Day/Night Cycling in Perovskite Solar Cells. *Energy Environ. Sci.* **2017**, *10*, 604–613.

(49) Domanski, K.; Alharbi, E. A.; Hagfeldt, A.; Grätzel, M.; Tress, W. Systematic Investigation of the Impact of Operation Conditions on the Degradation Behaviour of Perovskite Solar Cells. *Nat. Energy* **2018**, *3*, 61–67.

(50) Prochowicz, D.; Sasaki, M.; Yadav, P.; Grätzel, M.; Lewiński, J. Mechanoperovskites for Photovoltaic Applications: Preparation, Characterization, and Device Fabrication. *Acc. Chem. Res.* **2019**, *52*, 3233–3243.

(51) Hong, L.; Milić, J. V.; Ahlawat, P.; Mladenović, M.; Kubicki, D. J.; Jahanabkhi, F.; Ren, D.; Gélvez-Rueda, M. C.; Ruiz-Preciado, M. A.; Ummadisingu, A.; Liu, Y.; Tian, C.; Pan, L.; Zakeeruddin, S. M.; Hagfeldt, A.; Grozema, F. C.; Rothlisberger, U.; Emsley, L.; Han, H.; Grätzel, M. Guanine-Stabilized Formamidinium Lead Iodide Perovskites. *Angew. Chem., Int. Ed.* **2020**, *59*, 4691–4697.